Balance measurements on a frigate type ship model

Rafael Bardera[1] and Adelaida Garcia-Magariño[1]
[1]Instituto Nacional de Técnica Aeroespacial, 28850 Torrejón de Ardoz, Madrid, Spain

ABSTRACT

Balance measurements performed by testing sub-scaled ship models determine the global forces and moments acting on the ship, which allows knowing the power required for the ship's movement and provides insight to be applied in the design of the control systems used to steer the ship and to avoid instabilities while sailing.

The ship superstructure may produce large separated regions and high air wake turbulence levels resulting in a set of fluctuations of the flow parameters usually determined by measuring velocity or pressure. This paper presents the balance measurement of the aerodynamic forces acting on the ship hull. Aerodynamic forces and moments produced on the ship can be interpreted as an integration of the flow parameters (velocity and pressure distributions) over the ship surface wetted by the air. Balance method provides averaged values and fluctuations of forces coefficients.

Aerodynamic environment in the vicinity of a ship is influenced by a large number of factors (atmospheric wind, sea state, ship superstructure, masts, stacks, antennas…) affecting helicopter operations on board ships and their safety during the take-off and landing manoeuvres.

Keywords: forces and moments, ship stability, flight deck, air wake, balance measurements, balance spectra

1. Introduction

Global actions over the ship’s hull are the forces and moments which are experimentally measured by means of balances. The loads acting on the ship have effect on the required power for the ship motion and for its stability during the ocean navigation.

Usually, measurement campaigns are carried out in water channels to determine the hydrodynamic forces and moments that are exerted on the part of the ship that is underwater, for different navigation configurations.

Although the density of air is much lower than that of water, and consequently the aerodynamic loads are much less than the hydrodynamic ones, it is also interesting to determine the aerodynamic actions on the ship, which have effects on the part above the waterline, since they contribute to the consumption of mechanical power provided by

the power plant of the ship when they are against the advance of the ship.

Apart from this, the most important effect due to the aerodynamic actions is that can cause oscillations and instabilities on the ship during navigation. That is justified, for example, by analyzing the case of crosswind navigation, when the effects of the wind produce loads that results into a roll-over moment on the ship that will have to be compensated to guarantee the integrity and safety of the ship and the crew. Additionally, the knowledge of these aerodynamic actions will allow a more robust design of the control systems to avoid instabilities produced during the navigation of the ship.

On the other hand, the global aerodynamic forces acting upon the ship are a consequence of the local forces exerted on its surfaces which are determined by the air flow field around the ship. The flow field around the ship has been studied during the last decades because of its interaction with the operations of aircraft onboard.

Shipboard helicopter operations are performed in a very adverse and turbulent environment. Ship superstructure produces large separated regions and high air wake turbulence levels, so that, the airflow above the ship's flight deck is characterized by complex flow structures having very adverse effects on aircraft operations at sea (Findlay and Ghee 2006).

The flow field over the flight deck is largely dependent on the ship landing platform structure, commonly a bluff body, having a massive separated flow-region in its wake (Platt 1998). Figure 1 shows the typical flow encountered on the flight deck, similar to that of a backwards facing step with a closed recirculation zone bounded by an unsteady shear layer emanating from the top of the hangar and reattaching on the flight deck (Greenwell and Barret 2006). As observed in Figure 1, the flow incoming from the roof and the sides of the ship to the flight deck produces a large recirculation region behind the step thus causing counter-rotating vortices on each side of the recirculation region. This results in an unsteady horseshoe vortex structure (Zan 2001), that may grow, dissipate or move spatially in an unpredictable manner (Shafer and Ghee 2005).

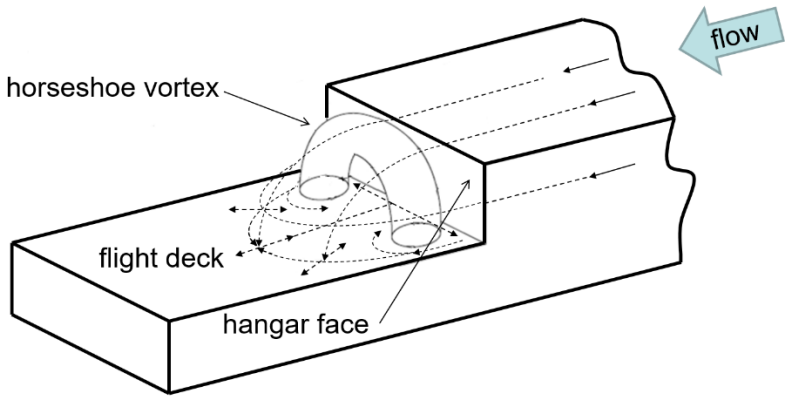

Figure 1. Three dimensional flight deck flow field.

The flow field on some general type of ships as the “Simple Frigate Ship” (Bardera-Mora 2014a) or the “Generic Frigate Ship” (Kääriä et al 2012) have been investigated by wind tunnel testing, in order to obtain information of a general ship geometry to establish comparative analysis with computational simulations as the case presented by Yuan et al. (2018).

The interaction of the atmospheric wind and sea state with the ship creates the operational environment for the helicopter, resulting in a slightly different flow for every type of ship (Geyer et al 2003). Regarding to this aspect, several computational and experimental studies were performed on specific ship geometries, such as the US Navy Destroyer DDG (Polsky et al. 2007) or some others (Bardera-Mora 2018a). Finally, a specific frigate was also investigated in wind tunnel by means of PIV (Bardera-Mora 2014b) and LDA (Bardera-Mora 2015 and 2017) and compared to on-board measurements used for validation the experimental and numerical results.

In order to study the flow field in the recirculated region on the flight deck and the flow frequencies involved that affect helicopters operation, wind tunnel test experiments have been performed. The most common non-intrusive experimental techniques for measuring the flow field velocity is the Particle Image Velocimetry (PIV) (Bardera and Meseguer 2015, Bardera-Mora et al 2017, Bardera-Mora et al 2018), which allows the obtention of velocity maps in this region, and the Laser Doppler Anemometry (LDA) (Bardera-Mora 2015 and 2017), which leads to the calculus of the flow frequencies involved, which are extremely important to know the pilot workload. Other classical techniques such as oil film visualization of the deck (Bardera-Mora 2014a) or pressure measurements (Buonaccorso et al. 2011, Bardera and Meseguer 2015) have also been employed.

On the other hand, some recent studies have proposed either some aerodynamic modifications (Kääira et al 2013 and Bardera et al 2015) or passive flow control devices (Findlay and Ghee, 2006, Bardera-Mora et al 2016) in the superstructures to reduce the turbulence level. However, neither of them have been applied by the ship manufacturers.

Recently, an instrumented model-scaled helicopter for measuring unsteady aerodynamic loading in ships airwakes, known as AirDyn, have been developed (Wang et al 2011) and used to compare to CFD results (Kääriä et al 2012). Also, a rotor flight simulation by CFD computations was performed to obtain an assessment of rotor-ship coupling effects (Tang et al. 2012).

In this context, wind loads acting on the ship model were measured in this work by means of a strain gauge balance as global aerodynamic forces and moment coefficients acting on the ship model.

Additionally, the spectral analysis of the balance signal provides the frequencies forcing the ship model structure. The frigate used in this work is the one used in Bardera et al (2015) and the frequencies obtained are compared to the main vortex shedding frequencies in the wake of the frigate model, as obtained previously by LDA measurements, showing good agreement.

2. Material and Methods

2.1. Wind tunnel

The experiments were conducted in a low-speed wind tunnel at INTA (Spain). The wind tunnel used is a close-circuit tunnel type with an open test section of 2 × 3 m^2, and a maximum airspeed of 60 m/s. Different wind velocities from 5 to 60 m/s were tested to reproduce different Reynolds numbers in the wind tunnel flow.

The wind tunnel has a platform with streamlined leading and trailing edges to minimize the interference of the platform in the flow field. In this case, this platform simulates the surface of the sea and the model only represents the part of the ship above the waterline subjected to aerodynamic air flow.

Figure 2 shows the ship model on the platform located in the test section of the wind tunnel.

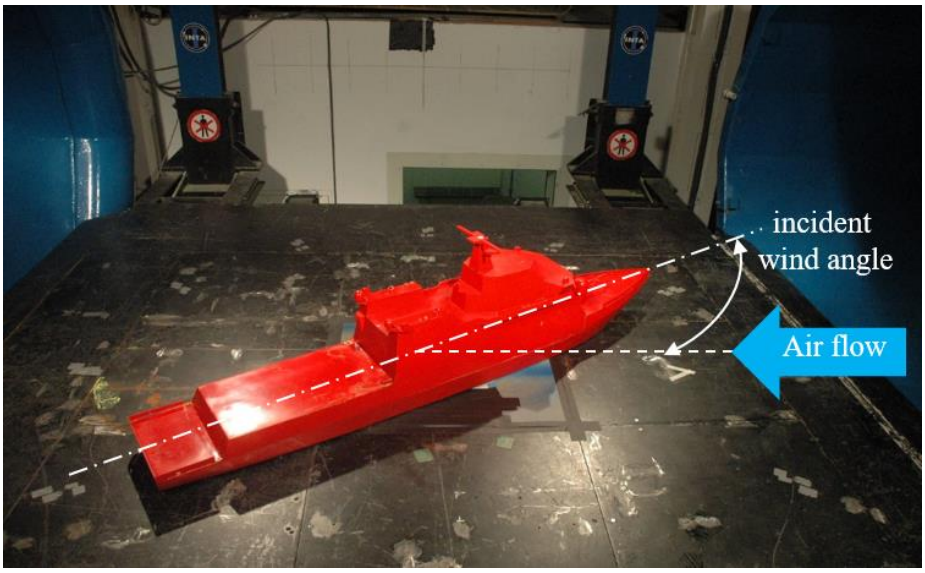

Figure 2. Ship model in the wind tunnel test section.

2.2. Ship model

The ship model used in this study is a scaled 1:50th specific frigate, with a flight helicopter deck located on the stern, where helicopters operate. The ship model has a hangar in the superstructure for helicopters. The superstructure also includes the bridge, radars, antennas and the exhaust funnels.

The most representative details of the ship model construction are given in Figure 3, where all dimensions are in millimetres.

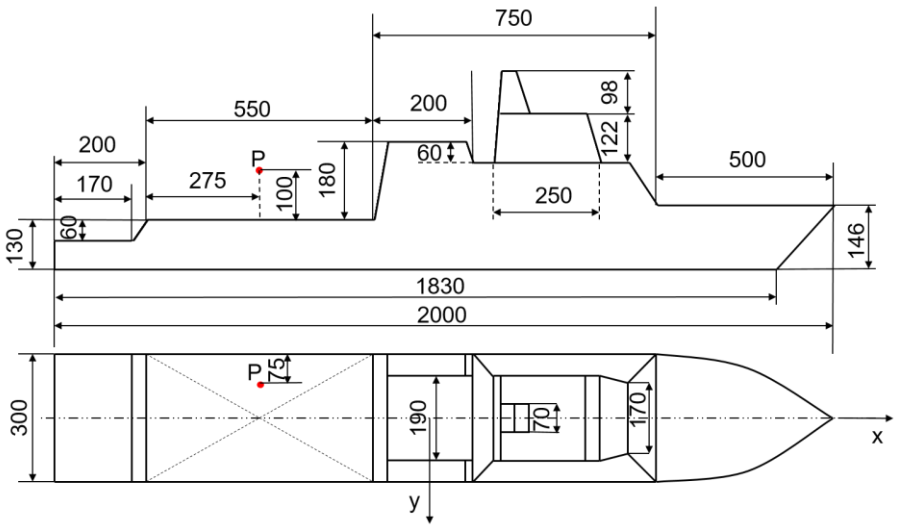

Figure 3. Ship model sketch (dimensions in mm).

2.3. Balance measurements

Balance measurement is a classical wind tunnel technique used for a global assessment of the wind loads acting over vehicles or buildings. Balances are usually fabricated with high tensile steel, operating in the elastic range of deformation, so that, when the loads stop, the balance material comes back to the original position without plastic deformation. When the balance is loaded, strain gauges installed over the balance get a measure of deformation and produce an electric signal. As the strain gauges are connected to a Wheatstone bridge, the unbalanced electric signal provides a measurement of the balance deformation which can be related with the load that produced this deformation.

For this experiment, a six-components strain gauge balance, FX2.6 SIXAXES model (Orlhac 2009) was installed outside the model, as an external balance, to measure the aerodynamic forces and moments acting on the ship model. Balance was calibrated before proceeding with the tests following the calibration procedure provided by the manufacturer (Orlhac 2009).

The ship model was fastened to the balance face by means of four screws in a classical manner of wind tunnel models in this kind of tests.

Balance measurements are expressed in the axes balance, with origin fixed to the balance centre of gravity. Figure 4 depicts the axes system associated to the balance, where X is the wind velocity direction, positive upstream, the Z axis is the vertical axis,

positive upward, and the Y-axis is perpendicular to both, X and Z axes, and directed according to the right-hand rule, so positive starboard, as shown in Figure 4. The balance centre of gravity was located 35 mm below the base of the ship model.

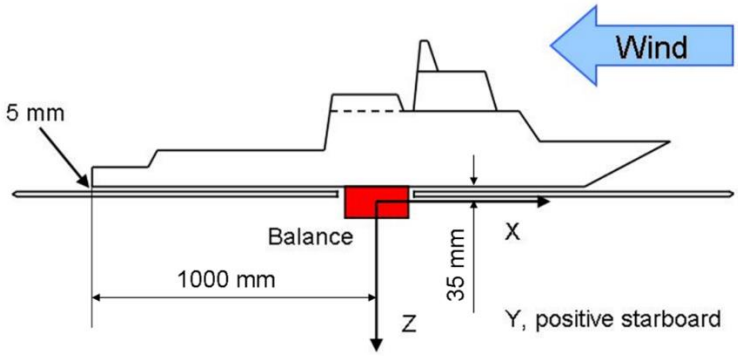

Figure 4. Balance system of axes

The model was fixed to the balance allowing a small gap (5 mm height) between both, platform and model base. No contact between the model and the platform was assured to avoid fictitious forces and moments in case deformations and vibrations occurred. In addition, the balance was fastened to an electro-mechanic rotary system allowing the model to rotate around the Z axis. This mechanism allows angles between 0º (bow-wind) and 180º (stern-wind), so different incident wind angles are possible during the test campaign.

2.3.1. Data acquisition

Figure 5 shows the components of the balance measurement system sketch. Balance was fed with a regulated power supply and data were acquired and recorded by using Quantum X software of HBM (Hottinger Baldwin Messtechnik GmbH).

The data acquisition of the balance was performed automatically at a sampling frequency of 2400 Hz, large enough to detect the present frequencies in the airflow. A low-pass Butterworth filter with cut-off frequency of 500 Hz was used to avoid aliasing, and the recording time was 16 seconds, considered both, sampling frequency and recording time, as adequate to get a correct signal reconstruction following the Nyquist-Shannon-Kotelnikov theorem applied to a discrete sequence of samples of a real continuous-time process.

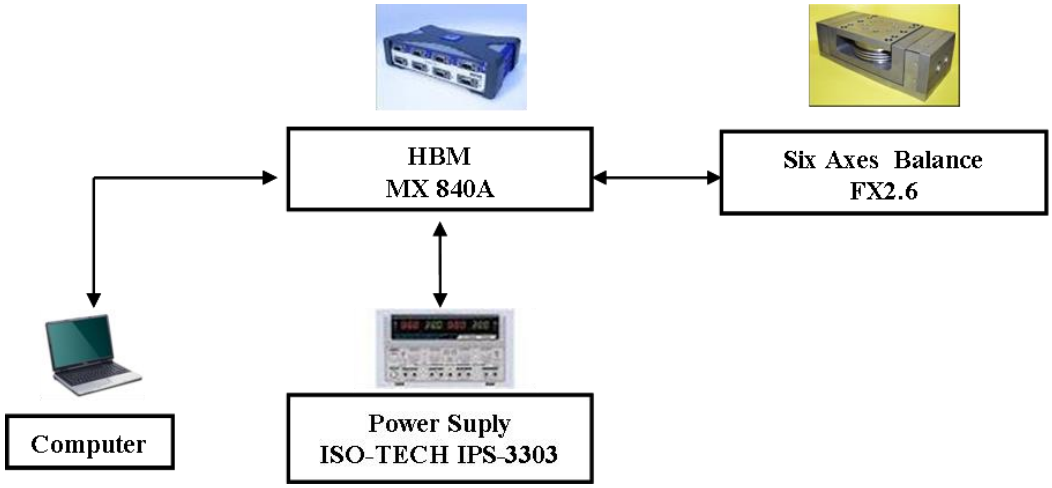

Figure 5. Balance measurement system sketch.

Values of forces and moments measurements have been averaged on the acquisition time, so that mean force and moment measured by the balance are given by the following expression,

$$[F]=[V][C] \tag{1}$$

where [*F*] is the force and moment matrix, [*C*] is the calibration matrix previously determined by means of calibration tests and [*V*] is the matrix of signals output corrected for zero offsets.

Matrix [*V*] is given by the following expression,

$$[V]=[V_r]-[V_0] \tag{2}$$

where [*Vr*] is the signals output readings matrix and [V_0] is the signals output zero offsets matrix (averaged of the initial and final zero offset).

Finally, the corresponding non-dimensional coefficients of force and moment are calculated by,

$$C_{Fi}=\frac{F_i}{q\cdot A} \qquad (i = x, y, z) \tag{3}$$

$$C_{Mi}=\frac{M_i}{q\cdot A\cdot L} \qquad (i = x, y, z) \tag{4}$$

where, C_{Fi} and C_{Mi} are the coefficients of force and moment, respectively, along the *"i"* balance axis *(i = x, y, z)*, F_i and M_i are the force and moment along the *"i"* balance axis, respectively and A is the reference surface (A = 0.094 m^2), taken as the front surface for zero incident wind angle. L is the reference length, (L is the beam when $i = x, z$ and the whole length of the ship model when $i = y$), and q is the dynamic pressure given by,

$$q = \frac{1}{2} \cdot \rho \cdot U_{\infty}^{2} \tag{5}$$

where ρ is the air density and U_{∞} is the free-stream velocity at the wind tunnel test section.

Finally, an axes rotation matrix allows changing from forces coefficients measured on axes fixed to balance (body axes) to wind axes forces, as given by the following expression (Barlow et al 1999),

$$C_{\bar{F}_w} = \begin{Bmatrix} C_{F_{X-w}} \\ C_{F_{Y-w}} \end{Bmatrix} = \begin{Bmatrix} -C_D \\ C_S \end{Bmatrix} = \begin{bmatrix} \cos\phi & \sin\phi \\ -\sin\phi & \cos\phi \end{bmatrix} \begin{Bmatrix} C_{F_X} \\ C_{F_Y} \end{Bmatrix} \tag{6}$$

where only X and Y components are to be accounted for, w indicates wind axes, C_D and C_S are the aerodynamic drag and side forces coefficients and C_{FX} and C_{FY} are the forces coefficients along the x and y-axes fixed to the balance, respectively. The incident wind angle is denoted as ϕ.

Force and moment measurements from the balance located at the base of ship model, experienced value fluctuations and the analysis of the signal spectra allowed the determination of the involved frequencies. The spectra were calculated by means of the Fourier Transform of the balance signals, using the FFT algorithm (Fast Fourier Transform). The dynamic balance response was previously calibrated by a step-response test, following an analogous procedure to that exposed in (Tanno et al. 2005).

3. Results

3.1. Balance measurements results

The main results obtained from the balance measurements are presented in graphical form. Figure 6 shows drag and side force coefficients versus incident wind angle when the wind tunnel velocity was 30 m/s and a Reynolds number Re = 5.5 × 10^5. For an incident wind angle of 90º, the drag coefficient has a maximum ($CDmáx$ = 3.8) and the side force coefficient is zero in wind axes ($CS = 0$). The drag coefficient for 0º is 0.6 ($CD(0º)$ = 0.6) and approximately, the same as the 180º case.

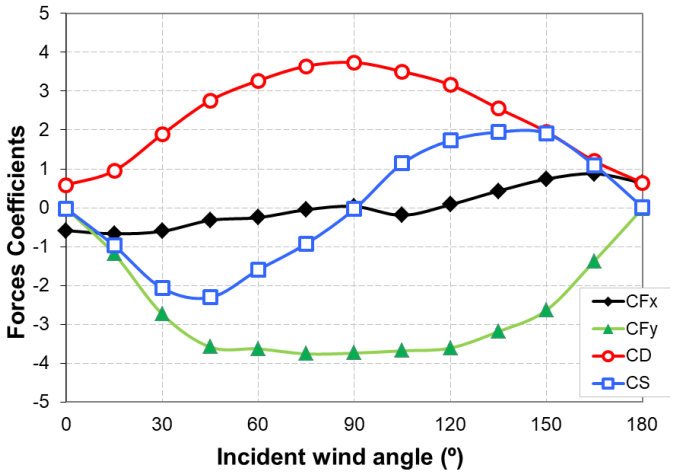

Figure 6. Aerodynamic forces coefficients vs incident wind angle.

Figure 7 shows moment coefficients expressed in balance axes versus incident wind angle when the Reynolds number is 5.5×10^5. When the incident wind angle is in the range from 45º to 120º C_{Mx} is approximately constant (C_{Mx} = - 2). This is the moment affecting the rolling attitude of the ship that is usually compensated by a great mass of water located in the ship hold as a dead weight.

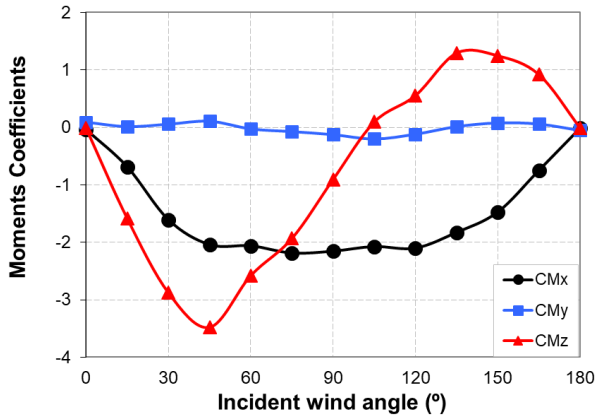

Figure 7. Moment coefficients vs incident wind angle.

Figure 8 shows aerodynamic drag force coefficient (C_D) versus flow Reynolds number (Re) for different incident wind angles. Graph indicates that drag force coefficient C_D is approximately independent of the Reynolds number as long as Re is above 1.0×10^5, showing slight ripple for some angles of wind incidence until Reynolds is rising to 8.0×10^5.

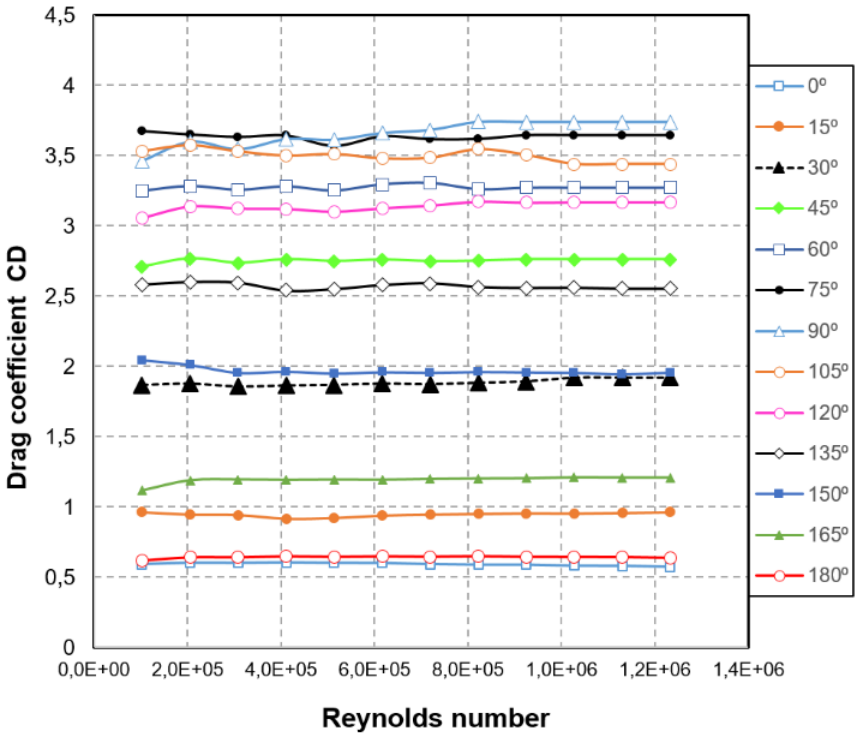

Figure 8. Drag coefficient versus Reynolds number.

The analysis of the balance signal spectra yielded the phenomenon frequencies. Power Spectral Density (PSD) of forces and moments was calculated from balance data following Press et al (2007). Spectra were estimated by time averaged periodograms, that were obtained by computing the Fast Fourier Transform (FFT), following the Welch's method (Welch, 1967), after the procedure detailed in Bardera-Mora et al., 2015.

Figure 9 shows the Power Spectral Density (PSD) of the forces *Fx* and *Fy* (spectra denoted by S_{Fx} and S_{Fy}). Forces were measured by means of the balance when wind tunnel velocity was 30 m/s, corresponding to a Reynolds number of 5.5×10^5. Horizontal axis represents the frequency values in Hz and vertical axis corresponds to the intensity of forces PSD in Newtons^2/Hertz.

The first peak of the spectrum, occurring at a frequency of about 10 Hz corresponds to the natural frequency of the ship model that was detected during a previous step-response test following an analogous procedure to that exposed in (Tanno et al. 2005) and without tunnel airflow when the model was joined to the balance. The model was loaded with a step load using a calibrated weight of 5 kg of mass in order to characterize it, which was hung from the model by a wire. The wire was cut at a certain moment to obtain the balance's response.

Taking into account that Strouhal number represents a non-dimensional frequency defined by $St = f \cdot L/U$, where f is the flow frequency, L is a body characteristic length

and U the flow velocity, the second peak that occurs at about 20 Hz corresponds to the hangar vortex shedding. Finally, several higher frequencies (50 to 70 Hz range) correspond to smaller devices such as the bridge, antennas and masts. Assuming the flow velocity U and the Strouhal number (St) are constant for bodies with similar geometry to a square cylinder, higher frequencies (≈ multiplied by 3) corresponds to smaller devices with lower sizes (≈ divided by 3).

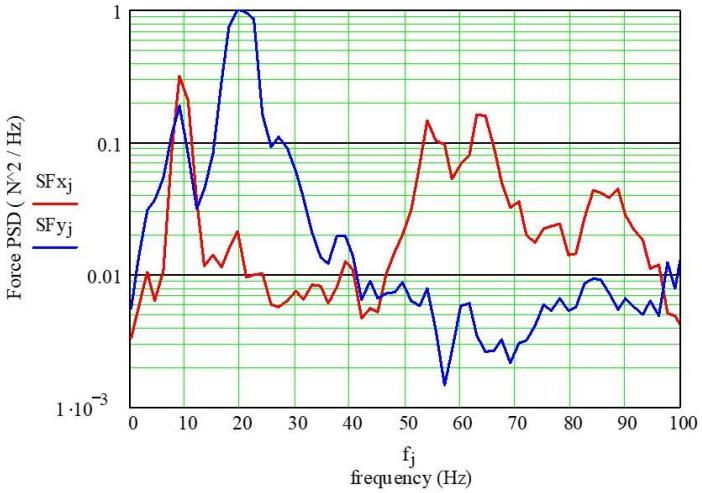

Figure 9. Power Spectral Density of aerodynamic forces.

Figure 10 shows the Power Spectral Density (PSD) of the balance moments signal (S_{Mx}, S_{My} and S_{Mz}) when freestream velocity of wind tunnel was 30 m/s (Re = 5.5×10^5). Now, vertical axis corresponds to the intensity of moments PSD in (Newtons × m)^2/Hertz.

The first peak of PSD spectrum corresponds to the natural frequency of the ship model (frequency of about 10 Hz) detected during the previous step-response test without airflow when the model was joined to the balance. The second peak of the spectrum is located about 20 Hz, probably, same as detected in the forces spectra (see Fig. 9), but the moment spectra exhibits very low signal level for harmonics into the frequency band from 50 to 70 Hz, so that, moment measurements results less sensitive for spectral analysis.

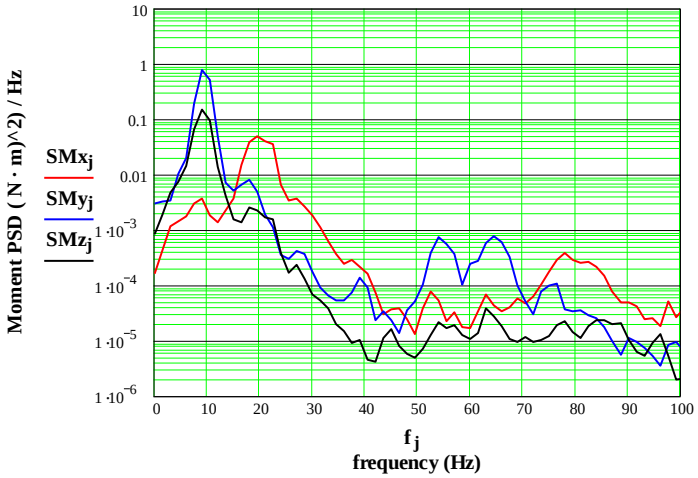

Figure 10. Power Spectral Density of the balance moments.

On the other hand, flow velocity was measured by means of Laser Doppler Anemometry (LDA) inside the air wake on the spot P (see Fig. 3). The LDA used is a commercial system from DANTEC). It consisted of a continuous 10 mW He-Ne laser, a BSA-F60 Flow Processor, the BSA Flow Software and a Laskin atomizer to seed the flow. This atomizer generates olive oil droplets with a diameter of the order of one micron, which are small enough to follow the flow.

Figure 11 shows the wind velocity spectrum of *v* component (along *y* axis), denoted by *Svv* following the results shown in reference Bardera-Mora et al 2015. Peak frequency obtained in this experiment was 17 Hz when testing at wind tunnel airspeed of 20 m/s, in the most representative point, spot P indicated in Fig. 3 (spot P2 in the reference).

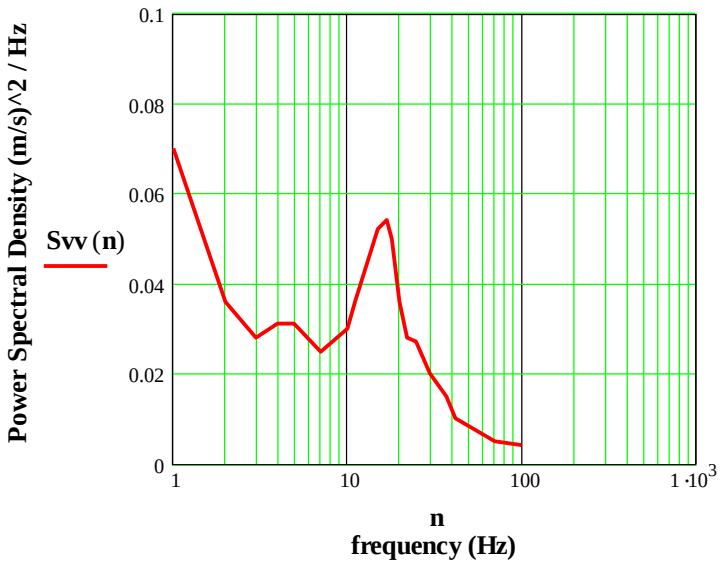

Figure 11. Power Spectral Density of wind velocity.

Figure 12 shows the Power Spectral Density (PSD) comparison between the balance signal and the flow velocity into the airwake as measured by LDA. The *y* component (indicated in Fig. 3 and 4) was represented in both cases, force *Fy*, moment *My* and velocity *v* component.

Flow velocity PSD denoted as *Svv* represents the kinetic energy divided by frequency, with units in International System (IS) of $(m/s)^2/Hz$. On the other hand, force PSD denoted by *SFy* in N^2/Hz is shown in vertical axis joined to *SMy* $(N \times m)^2/Hz$ and *Svv.*

As observed in Figure 12, the force spectrum exhibits more intensity than flow velocity spectrum, but they are different quantities, with different physics units. The force spectrum has a main frequency peak located at 20 Hz. On the other hand, moment spectrum shows two peaks, the first one is due to natural frequency of the model and it is located at 10 Hz, and the second peak is located at 18 Hz, close to the peak detected in the velocity spectrum, located at 17 Hz. Higher frequencies show the turbulent kinetic energy, represented by *Svv*, is decaying as expected in a turbulent flow, and Figure 11 shows how it trends to the force spectrum curve (see Fig. 11 and 12).

Frequency peak at 17 Hz, detected in flow velocity spectrum corresponds to the hangar vortex shedding frequency same as found in a previous work (Bardera-Mora et al. 2015). This value is near the force spectrum frequency of 20 Hz. Discrepancies found could be due the small differences found in the Reynolds number, since as shown before, the independency of the Reynolds number is not fully attained until Reynolds above 8.0×10^5.

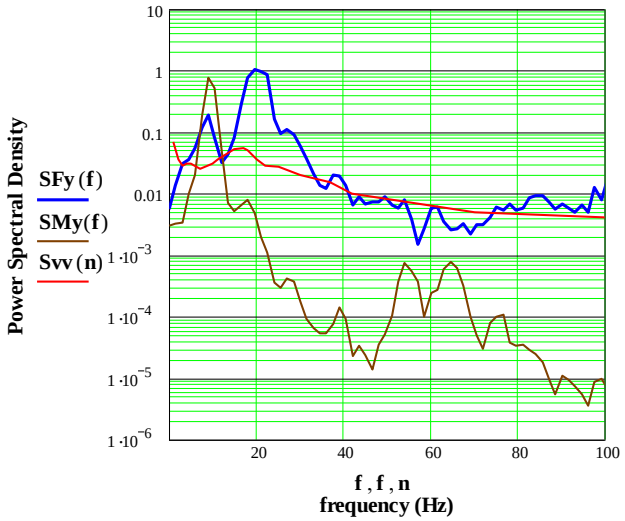

Figure 12. Power Spectral Density comparison.

4. Conclusions

A sub-scaled model of a frigate type ship was built and tested in a low-speed wind tunnel in order to perform force and moment measurements by means of a strain gauge balance located in the base of the ship model. Corresponding force and moment coefficients were calculated and plotted. Additionally, the variation of the drag coefficient with Reynolds number of the flow was studied, showing Reynolds number independency when the flow Reynolds number is above 1.0×10^5 with some slight ripple for some incident wind angles until 8.0×10^5. Consequently, the wind tunnel test reproduces adequately the full-scale ship airflow structure at Reynolds number of order of 1.0×10^7.

Roll moment coefficient was determined as a relative wind angle function (0 to 180º range). An estimate of the roll moment on the full-scale ship can be calculated using this coefficient and consequently the dead load to equilibrate it.

The analysis of the balance signal spectra allowed the determination of the main frequencies affecting to the ship model structure as these located around 20 Hz, and other secondary peaks in the range from 50 to 70 Hz with a very low intensity.

The frequencies present in the flow were determined from wind velocities measured by means of Laser Doppler Anemometry. The spectrum exhibits the classical shape of turbulent flow with typical decaying after higher peak located in 17 Hz for the studied flow. A comparative analysis of balance and LDA spectra reveals that LDA frequency peak is located closed to this of balance peak.

Finally, we can conclude that the balance measurements method provide information about the aerodynamics loads acting on the ship that can be used in the computation of

the required power for the ship's movement and improving the design of the control systems in order to steer the ship in a more safe manner maintaining the ship's stability while sailing. On the other hand, the analysis of the balance signal spectra has been proved to be valid to determine ship frequencies acting on the frigate ship tested.

Acknowledgments

This investigation has been funded by INTA, under the internal project "Termofluidodinámica".

References

Bardera-Mora, R. 2014a. Experimental investigation of the flow on a simple frigate shape (SFS). *The Scientific World Journal, 2014*.

Bardera-Mora, R. 2014b. Flow field velocity on the flight deck of a frigate. *Proceedings of the Institution of Mechanical Engineers, Part G: Journal of Aerospace Engineering*, *228*(14), 2674-2680. https://doi.org/10.1177/0954410014524739

Bardera-Mora, R., Barcala-Montejano, M. A., Rodríguez-Sevillano, A., de Diego, G. G., & de Soto, M. R. 2015. A spectral analysis of laser Doppler anemometry turbulent flow measurements in a ship air wake. *Proceedings of the Institution of Mechanical Engineers, Part G: Journal of Aerospace Engineering*, *229*(12), 2309-2320. https://doi.org/10.1177/0954410015573972

Bardera, R., Meseguer, J. 2015. Flow in the near air wake of a modified frigate. *Proceedings of the Institution of Mechanical Engineers, Part G: Journal of Aerospace Engineering*, *229*(6), 1003-1012. https://doi.org/10.1177/0954410014542449

Bardera-Mora, R., Barcala-Montejano, M. A., Rodríguez-Sevillano, A., & Nova-Trigueros, J. 2016. Passive flow control over the ski-jump of aircraft carriers. *Ocean Engineering*, *114*, 134-141. https://doi.org/10.1016/j.oceaneng.2016.01.019

Bardera-Mora, R., León Calero, M., & García-Magariño, A. 2017. Aerodynamic effect of the aircraft carrier island on flight deck flow with cross wind. *Proceedings of the Institution of Mechanical Engineers, Part M: Journal of Engineering for the Maritime Environment*, *232*(2), 145-154. https://doi.org/10.1177/1475090216689172

Bardera-Mora, R., Garcia-Magariño, A., Rodríguez-Sevillano, A., & Barcala-Montejano, M. A. 2018. Aerodynamic Flow Effects on Aircraft Carrier Takeoff Performance. *Journal of Aircraft*, 1-9. https://doi.org/10.2514/1.C035188

Barlow, J. B., Rae, W. H. Jr. & Pope, A. "Low-Speed Wind Tunnel Testing", 3rd Edition. John Wiley & Sons, Inc. USA 1999.

Buonaccorso, J., Widma, S. and Miklosovic, D., Pressure Field Mapping of a Modified YP Craft Flight Deck. AIAA Centennial of Naval Aviation Forum “100 Years of Achievement and progress”, 21-22 September 2011, Virginia Beach, VA. AIAA 2011 - 7044.

Findlay, D. B., Ghee, T., 2006 “Experimental Investigation of Ship Air wake Flow Control for US Navy Flight II-A Class destroyer (DDG)”.AIAA 2006-3501. 3rd AIAA Flow Control Conference 5-8 June 2006, San Francisco, California.

Geyer, W. P., Long, K. & Carico, D. “Helicopter/Ship Qualification”. Part 2: American Clearance Process. RTO AG-300 Vol. 22/SCI-038. RTO/NATO 2003. ISBN 92-837-1093-2.

Greenwell, D. I. & Barrett, R. V., “Inclined Screens for Control of Ship Air Wakes”, *AIAA 2006-3502*, 3rd AIAA Flow Control Conference 5 - 8 June 2006, San Francisco, California.

Kääriä, C. H., Wang, Y., Padfield, G. D., Forrest, J. S., & Owen, I. 2012. Aerodynamic loading characteristics of a model-scale helicopter in a ship's airwake. *Journal of Aircraft*, *49*(5), 1271-1278. https://doi.org/10.2514/1.C031535

Kääriä, C. H., Wang, Y., White, M. D., & Owen, I. 2013. An experimental technique for evaluating the aerodynamic impact of ship superstructures on helicopter operations. *Ocean engineering*, *61*, 97-108. https://doi.org/10.1016/j.oceaneng.2012.12.052

Oppenheim, A. V., Willsky, A. S. “Signals and Systems”. Second Edition. Prentice Hall International Inc., 1997

Orlhac A.; Balance FX2.6 Sixaxes. *Dossier D64059-SAV-E*.

Platt, J. R., Wind Detection in a Microcosm: Ship/Aircraft Environment Sensors. *IEEE AES Systems Magazine*, February 1998.

Polsky, S., Imber, R., Czerwiec, R., Ghee, T., A Computational and Experimental Determination of the Air Flow Around the Landing Deck of a US Navy Destroyer (DDG): Part II. 37th AIAA Fluid Dynamics Conference and Exhibit, 25-28 June 2007, Miami, FL. AIAA 2007 - 4484.

Press W. H., Teukolsky, S. A., Vetterling W. T., Flannery B. P., 2007 “*NUMERICAL RECIPES, The Art of Scientific Computing”*. Third Edition. Cambridge University Press 2007, UK.

Shafer, D. M., Ghee, T. A. “Active and Passive Flow Control over the Flight Deck of Small Naval Vessels”. *AIAA 2005-5265*. 35th AIAA Fluid Dynamics Conference and Exhibit 6-9 June 2005, Toronto, Ontario, Canada.

Tang, L., Dinu, A., Polsky, S., Reduced-Order Modeling of Rotor-Ship Interaction, 50th AIAA Aerospace Sciences Meeting including the New Horizons Forum and Aerospace Exposition, 09 - 12 January 2012, Nashville, Tennessee. AIAA 2012-1300.

Tanno, H., Itoh, K., Komuro, T., Sato, K. Ueda, S. "Design and Evaluation of Strain Gauge Force Balance with Short Test Duration". Trans. Japan Society for Aeronautical Sciences Vol. 48. No. 159, pp. 1-6, 2005.

Wang, Y., Curran, J., Padfield, G. D., & Owen, I. 2011. AirDyn: an instrumented model-scale helicopter for measuring unsteady aerodynamic loading in airwakes. *Measurement Science and Technology*, *22*(4), 045901. https://doi.org/10.1088/0957-0233/22/4/045901

Watson, N. A., Kelly, M. F., Owen, I., Hodge, S. J., & White, M. D. 2019. Computational and experimental modelling study of the unsteady airflow over the aircraft carrier HMS Queen Elizabeth. *Ocean Engineering*, *172*, 562-574. https://doi.org/10.1016/j.oceaneng.2018.12.024

Welch, P. D., The Use of Fast Fourier Transform for the Estimation of Power Spectra: A Method Based on Time Averaging Over Short, Modified Periodograms. IEEE Transaction on Audio and Electroacoustic, June 1967. Pp. 17-20.

Yuan, W., Wall, A., Lee, R., Combined numerical and experimental simulations of unsteady ship airwakes. Computers & Fluids, Vol. 172, 30 August 2018, pp. 29-53.

Zan, S. J. "Surface Flow Topology for a Simple Frigate Shape", *Canadian Aeronautics and Space Journal*, Vol. 47, No. 1. 2001.